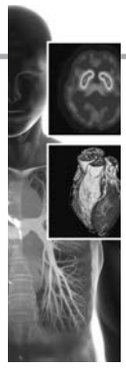

Functional MRI for tumor delineation in prostate radiation therapy

A unique property of radiation therapy is the capacity for a differential treatment, in which a high dose can be delivered to tissue with a high tumor load, whereas a lower dose is applied to treat microscopic disease around the primary tumor. This approach is termed 'dose painting' and is currently tested in the radiation therapy of prostate cancer. Functional MRI techniques, such as dynamic contrast-enhanced MRI and diffusion-weighted MRI, are well established for tumor localization and staging. However, application for target delineation in radiotherapy raises some specific issues: at what spatial resolution can these techniques be used reliably? What is the detection limit of the techniques? Do different techniques identify the same regions as suspicious or do they provide complimentary information? In this article we address these issues and explore how functional MRI techniques can be used for radiotherapy dose painting.

KEYWORDS: DCE-MRI ■ diffusion-weighted MRI ■ dose painting ■ dynamic contrast-enhanced MRI ■ MRI ■ prostate ■ radiotherapy ■ tumor delineation

Uulke A van der Heide†1, Johannes G Korporaal1, Greetje Groenendaal1, Stefan Franken1 & Marco van Vulpen1

1Department of Radiotherapy, University Medical Center Utrecht, Heidelberglaan 100, 3584 CX Utrecht, The Netherlands
†Author for correspondence:
Tel.: +31 887 557 209
Fax: +31 887 555 850
u.a.vanderheide@umcutrecht.nl

Radiation therapy is one of the primary treatment modalities for localized and locally advanced prostate cancer. In the absence of precise information about the location of cancerous tissue inside the prostate, the conventional approach has been to treat the entire gland to a more or less homogeneous dose. In several randomized trials it has been shown that escalation of the radiation dose to the prostate benefits the outcome. Up to now, several randomized trials [1–3] have showed an increase in 5-year biochemical freedom from relapse in locally advanced disease from approximately 50 to 65% when increasing the external beam radiation dose from 68 to 78 Gy. Current modern techniques, such as intensity modulated radiation therapy in combination with position verification, based on fiducial markers in the prostate, enable a safe delivery of such high doses, whilst avoiding an increase in treatment-related toxicity and a clinically relevant deterioration in quality of life [4,5].

Even further dose escalation is expected to have an additional benefit on treatment results, as evidence emerges that local recurrences are mostly found at the location of the primary tumor [6,7]. However, in particular at the dorsal side of the prostate, such a dose escalation is in conflict with the constraints required to limit rectum toxicity. For this reason, several groups have proposed limiting the boost of the radiation dose to the visible dominant lesion inside the prostate [8–11], following an approach that is termed 'dose painting' [12]. Here, a unique property of radiation therapy is exploited that distinguishes it from other treatment modalities. Radiation therapy has the capacity for differential treatment, in which a high dose can be delivered to treat a dominant lesion in the prostate, whereas the remainder of the gland is irradiated with a lower dose to treat microscopic disease. This capacity sets it apart from all-or-nothing therapies, such as surgery and cryotherapy [13].

Dose painting is now being tested in clinical practice for the treatment of prostate cancer. Two studies reported on the acute toxicity of dose escalation to the dominant intraprostatic lesion of 82 Gy [14] and 95 Gy [15]. In both studies, observation of severe toxicity (CTC toxicity score [16] equal to or greater than grade 3) was minimal. Recently, a randomized Phase III trial started to investigate the benefit of a Focal Lesion Ablative Microboost (FLAME) trial, escalating the dose to the tumor from 77 Gy in the standard arm to 95 Gy in the study arm [101]. In both arms, the dose to the remainder of the prostate is kept to 77 Gy. In the FLAME trial, the tumor inside the prostate is delineated based on a combination of anatomical and functional MRI (fMRI) sequences (Figure 1 & Table 1).

The effectiveness of dose painting in the prostate relies on the high sensitivity and specificity of the imaging techniques used to visualize the tumor. T_2-weighted MRI can be used for this purpose. The sensitivity and specificity of tumor detection increases when this modality is combined with dynamic contrast-enhanced MRI (DCE-MRI), diffusion-weighted MRI (DWI) or magnetic resonance spectroscopic imaging

future medicine part of fsg

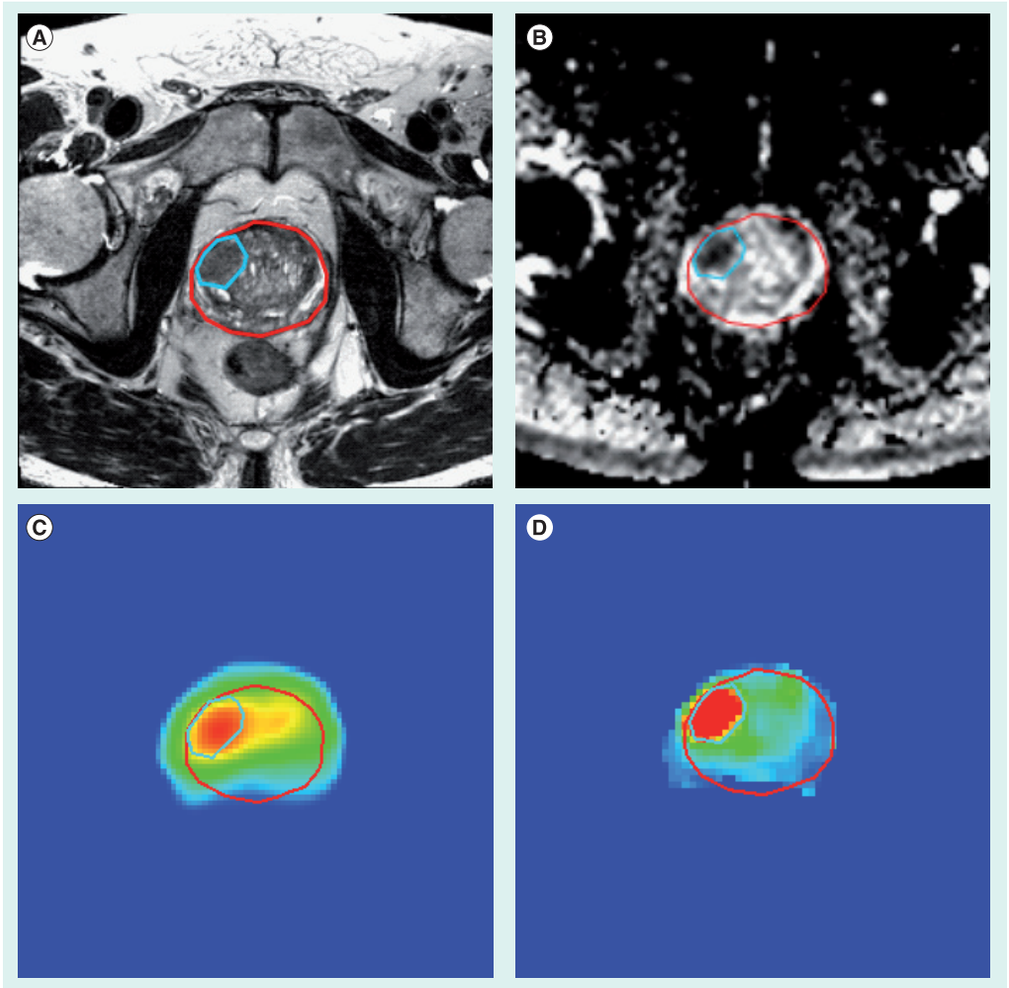

Figure 1. Dose painting in the FLAME trial based on T_2-weighted MRI (A), an apparent diffusion coefficient map, obtained from diffusion-weighted MRI (B), and a K^{trans} parameter map derived from dynamic contrast-enhanced MRI (C), with dose distribution shown in (D). Imaging and dose parameters for the gross target volume and remainder of the prostate are shown in Table 1.

(MRSI). However, while the application of these imaging techniques provides great opportunities for tumor delineation in radiotherapy, it also presents some specific challenges. For a precise delineation of the tumor, images of a sufficiently high spatial resolution must be available. For functional imaging modalities, the spatial resolution at which parameter maps can be interpreted must be established. The use of multiple imaging techniques may provide complementary information, which enhances the sensitivity and specificity of the examination in a diagnostic setting. However, if suspicious volumes in multiple imaging modalities show only a partial overlap, the question arises as to what to delineate as the target volume for irradiation.

Here, we present an overview of the use of MRI in the context of target delineation for radiation therapy of the prostate. First, we address the use of MRI for delineation of the prostate. After a brief overview of the fMRI techniques used for tumor detection and staging in the

Table 1. Imaging and dose parameters.

Parameter	GTV	Remainder prostate
Mean ADC (mm^2/s)	$0.93*10^{-3}$	$1.17*10^{-3}$
Mean K^{trans} (min^{-1})	0.85	0.18
Mean dose (Gy)	94.0	81.4

Imaging and dose parameters for the patient shown in Figure 1.
ADC: Apparent diffusion coefficient; GTV: Gross target volume.

diagnostic phase, we discuss issues that are particular for their application in tumor delineation. Finally, future developments that may have an impact on radiation therapy are discussed.

MRI for delineation of the prostate

The impact of MRI on the delineation of the prostate gland has been well established and reviewed [17]. Comparing the intra-observer variation with CT alone and with the combination of CT and T_2-weighted MRI, many groups found that the variation decreased substantially. In particular the position of the apex could be determined more consistently. Near the apex, on CT the prostate boundary tended to be delineated 3–5 mm more caudally than on MRI, resulting in an overestimation of the prostate volume with a factor of 1.3–1.4. To improve the quality of prostate delineation on T_2-weighted MRI, McLaughlin *et al.* reviewed the functional anatomy as well as their visibility on T_2-weighted MRI [18]. Villeirs *et al.* published a guide for radiotherapists using MRI in the treatment planning for prostate cancer [19]. They review structures seen in and near the normal prostate as well as well as in prostates with cancer.

Rosewall *et al.* demonstrated that MRI also improves the quality of prostate delineation in patients with bilateral hip prostheses, where CT images suffer from artifacts [20]. In a study of seven patients, they found that the mean volume delineated by four radiation oncologists was 21% larger on CT than on MR, in line with the findings described above. The inter-observer variability also tended to be smaller, while the prostheses did not appear to cause measurable geometric distortions on the sequences used.

MRI for detection & staging of prostate cancer

The use of fMRI for staging of prostate cancer has been reviewed extensively [21–23]. While many studies show promising results about their diagnostic performance, a clear consensus about the use of these techniques is still lacking and the role of MRI in published guidelines is still quite limited. Nevertheless, MRI techniques are gaining recognition as an important tool for detection and localization of prostate tumors [23].

For T_2-weighted imaging alone, the staging accuracy varies considerably, with sensitivities ranging from 37 to 96% and corresponding sensitivities reported in the range between 21 and 67% [24]. The use of a 3T MRI and an endorectal coil results in an improvement of the sensitivity and specificity to 88 and 96% for experienced radiologists, while a less experienced radiologist reached values of 50 and 92%, respectively [25].

The performance of T_2-weighted MRI is improved when it is combined with DCE-MRI and MRSI [22]. DCE imaging with Gd-DTPA contrast agent reflects the properties of the vasculature, such as micro-vessel density and permeability of the vessels. The angiogenesis in tumors results in an increase in micro-vessel density, but also a highly disorganized capillary network. This is reflected in the different enhancement curves in prostate tumors and healthy tissue. A high sensitivity and specificity of tumor detection has been shown. Hara *et al.* uncovered 92.9% of the clinically significant cancers, with a specificity of 96.2% [26]. Kim *et al.* found a sensitivity and specificity of 96 and 82% for DCE-MRI, as compared with 65% and 60% for T_2-weighted MRI, respectively [27]. In the transitional zone the sensitivity of DCE-MRI was also 96%, compared with 45% for T_2-weighted MRI. However, the specificity was not significantly improved when compared with T_2-weighted MRI (51 vs 73%, $p = 0.102$). Using tracer-kinetics modeling with the Tofts model [28], Fütterer *et al.* found the highest accuracy for the model parameter v_e, representing the volume fraction of the extracellular extravascular space, with a sensitivity between 90 and 95% and a specificity between 85 and 88% [29].

Magnetic resonance spectroscopic imaging has a high specificity in the identification of tumors inside the prostate. Fütterer *et al.* found a sensitivity between 77 and 80% and a specificity of 84–87% [29]. A high ratio of choline and creatine to citrate is indicative of cancer. However, the spatial resolution of MRSI is relatively poor, making it more difficult to detect small lesions [30–31].

Diffusion-weighted MRI has been used extensively to study the random translational motion of water molecules. In tumors, the increased cellularity restricts water motion in a reduced extracellular space, thus causing a reduction of the apparent diffusion coefficient. In the prostate, DWI has been quite successful, with sensitivities and specificities well above 80% [32–39]. Yoshimitsu *et al.* showed that lower apparent diffusion coefficient (ADC) values also correlate with a higher Gleason score [37].

Combining fMRI techniques in one examination further improves the performance [23,25,29]. Seitz *et al.* point out that MRSI, DWI and DCE-MRI all deliver additional information to

morphologic changes depicted on T_2-weighted MR images [23]. They conclude that the combination of conventional MRI with fMRI techniques is more reliable for differentiating benign and malignant prostate tissue than any other diagnostic procedure.

Application of fMRI techniques in radiation therapy

The excellent performance of MRI techniques for tumor detection and staging creates the potential to apply these techniques for tumor delineation in radiation therapy. However, it is important to note that the diagnostic questions addressed in most studies are different from the questions that are relevant for tumor delineation. Studies reporting on the sensitivity and specificity of tumor detection mainly focus on the question if a patient has prostate cancer and only on the approximate location of that tumor. Studies regarding staging report on the accuracy of detecting capsular extension of the disease or involvement of the seminal vesicles. The answers to these questions have direct consequences for the choice of treatment. On the other hand, when patients are scheduled for radiation therapy, the presence of prostate cancer has been proven with biopsies and the stage of the disease has been established. Thus, rather than a qualitative assessment of location or capsular extension of the tumor, the precise boundaries of the lesions inside the prostate must be determined for target delineation.

■ Repeatability & spatial resolution

Delineation of a lesion within the prostate implies that for each voxel a decision has to be made as to whether it is part of the tumor or not. Therefore, it is important to know the smallest voxel size at which the parameter maps obtained from fMRI still retain meaningful information: the precision at which a parameter can be determined needs to be sufficient to distinguish values associated with tumors from values associated with healthy tissues. Image noise and day-to-day variation in a patient cause an uncertainty in these values. Both sources of uncertainty are reflected in the repeatability of a measurement, as quantified in the within-patient standard deviation.

While day-to-day variation in a patient is difficult to control, the signal-to-noise can be improved by increasing image voxels, at the cost of spatial resolution. For this reason, it is relevant to understand the relation between repeatability and voxel size: for small voxels the repeatability will be limited by image noise and may be insufficient for delineation of the tumor. For large voxels, the repeatability will mainly reflect day-to-day variations, but these voxels may be too large for delineation.

To date, results of voxel-wise repeatability in prostate cancer are lacking for fMRI techniques. The repeatability of fMRI techniques is addressed in only a few studies, mainly for the purpose of determining the detectable changes in functional parameters after treatment. In a study of 20 patients with prostate cancer, Alonzi *et al.* carried out two MRI examinations on subsequent days, prior to the start of treatment with androgen deprivation therapy [40]. The examination consisted of DCE-MRI as well as other fMRI techniques. The within-patient coefficient of variance (wCV) was determined for the entire prostate and regions of interest in the tumor, normal peripheral zone and transition zone. For these regions, with quite a variation in volume, wCV values were found between 13.9 and 41.9% for K^{trans}. From these data the threshold levels could be determined, beyond which a change in parameter could be considered a real change with a 95% confidence level. Similar numbers were reported for healthy structures and other tumors [41]. Kershaw *et al.* found wCV values for K^{trans} in healthy prostate tissue of 31 and 27% in the peripheral zone and central gland, respectively [42]. The wCV for healthy prostate T_2 values was 3%.

A key problem in the acquisition and analysis of DCE-MRI data is the accurate measurement of the arterial input function (AIF), needed for absolute quantification. Owing to the nonlinear relationship between the signal and contrast agent concentration and artifacts, such as T_2^*-effects, B1-field inhomogeneities and in-flow effects, the repeatability of AIF measurements tends to be poor with correlation of variance values of up to 50% in peak height and 25% in the tail of the AIF [43]. The impact of these variations is mostly a scaling of the tracer kinetics parameter map K^{trans}. It is clear that these difficulties have an impact on the repeatability of the DCE-MRI examination. Furthermore, it explains why between studies of different institutes large differences are found in the parameter range of K^{trans} in healthy (0.06–0.60 min^{-1}) and cancerous (0.18–1.26 min^{-1}) prostate tissue (**Table 2**) [44–50].

The challenges described above can be circumvented with DCE-CT, which has become feasible with multislice CT scanners that allow imaging of sufficiently large slabs at once [51]. Jeukens *et al.* investigated the impact of image

noise on the confidence intervals of tracer kinetics model parameters [52]. By integrating the signal in a volume of approximately 0.1 cc, noise levels could be obtained that allow for reliable tracer kinetics modeling. Korporaal *et al.* studied the repeatability of DCE-CT as a function of voxel size [53]. A group of 29 patients underwent two DCE-CT examinations within 1 week prior to radiation therapy. Parameter maps of K^{trans} and other parameters in the Tofts model were calculated at 15 different image resolutions. For the group of patients, the median K^{trans} in the suspected tumors was 0.24 min^{-1} and in the regions of interest in the healthy peripheral zone it was 0.11 min^{-1}. In a voxel-wise comparison between the two examinations, the within-voxel standard deviation was determined. The day-to-day variation of the DCE-CT examination was reflected in a wSD for K^{trans} of 0.027 min^{-1}, obtained from signals integrated in a voxel of 2.6 cc. For signals integrated in a volume of 0.15 cc, corresponding to a cube of 5.3 mm^3, a wSD of 0.047 was found. Thus, at this voxel size, the uncertainty in K^{trans} is sufficiently small to allow discrimination between values associated with tumor and healthy tissue. The precise implication of these results for MRI needs to be investigated. However, as the signal-to-noise in MRI should be higher than in CT, a spatial resolution similar to that found in DCE-CT should be feasible.

For diffusion-weighted imaging, the repeatability of examinations of the prostate was studied by Gibbs *et al.* in eight healthy volunteers [54]. The repeatability of the ADC values varied between 10 and 35%, depending on experimental conditions. The authors also showed the impact of signal-to-noise on the repeatability by varying the number of signal averages. Increasing the number of signal averages from 1 to 16, the repeatability improved from 10 to 4%. Varying the size of the region of interest from 0.3 to 1.7 cc seemed to have little impact on the repeatability.

Differences in methodology between institutions and quantification problems inherent to the acquisition limit the quantification of functional parameters. For DWI-MRI, researchers have proposed a consensus approach to address this issue [55]. For DCE-MRI the situation is not as clear. Although, in particular the Tofts model has contributed to the agreement about nomenclature and definitions in tracer kinetic modeling [28], there is still insufficient consensus about the standardization of DCE-MRI imaging protocols.

Table 2. Overview of dynamic contrast-enhanced MRI K^{trans} values (min^{-1}) for tumor and healthy peripheral zone in the literature, demonstrating the wide spread of values between institutes.

Healthy peripheral zone	Prostate cancer	Ref.
0.15 ± 0.08	0.28 ± 0.13	[44]
0.34 ± 0.17	0.59 ± 0.31	[30]
0.60 ± 0.56	1.26 ± 0.54	[45]
0.23 ± 0.25	0.47 ± 0.57	[46]
0.13	0.27	[47]
0.50, range 0.20–0.82	1.09, range 0.46–1.97	[48]
0.06 ± 0.03	0.18 ± 0.06	[49]
0.29, range 0.09–0.87	0.36, range 0.16–1.28	[50]

■ Use of an endorectal coil

The application of fMRI techniques for tumor delineation in the prostate poses specific challenges. The scan protocols that have been found to be optimal for prostate scanning typically involve the use of an endorectal coil owing to its superior signal-to-noise. In particular at 1.5T, the use of an endorectal coil, combined with a pelvic phased-array coil is recommended for diagnostic imaging [21]. At 3T the improved signal-to-noise ratio of the high-field-strength systems can compensate some of the signal loss when scanning with only a phased-array coil. Figure 1 & Table 1 show a good signal-to-noise for the T_2-weighted image scanned at 3T with a phase-array coil, yielding an in-plane resolution of 0.78 mm and a slice thickness of 3 mm. In addition, proton MR spectroscopy was shown to be feasible without an endorectal coil [56]. Nevertheless, Heijmink *et al.* demonstrated that the image quality of T_2-weighted images of the prostate improved significantly at 3T with the use of an endorectal coil when compared with a body array coil [57].

For radiotherapy, the deformation of the prostate by the endorectal coil is problematic, as it results in an image of the prostate that is not representative of the situation during the radiation therapy. Heijmink *et al.* studied the change in prostate shape by comparing 3T MRI images made with and without an endorectal coil [58]. They found an average decrease of the antero-posterior diameter of 5.5 mm after insertion of the endorectal coil. The mean right-to-left and cranio-caudal diameter increased by 3.5 and 2.2 mm, respectively. The mean volume of the prostate also decreased significantly by 17.9% for the total prostate, 21.6% for the peripheral zone and 14.2% for the central gland. These results are consistent with those found by Kim *et al.*, also demonstrating that an expandable coil caused more deformations than a rigid coil [59].

In a rather rigorous approach to deal with this problem, Van Lin *et al.* proposed to use a rectal balloon while making the planning CT scan and during all 35 radiation therapy treatment fractions [10]. While additional benefits of a rectal balloon are claimed, in particular for minimizing the radiation exposure of the rectal wall [60], the patient discomfort, as well as workload of this procedure, seems to prevent widespread use. An alternative is the use of nonrigid registration techniques to correlate MRI images made using an endorectal coil with planning CT images made without it. Alternatively, the use of a colorectal coil, rather than an endorectal coil, could be investigated in the hope that it would not cause large distortions of the prostate while yielding a high signal-to-noise. However, in practice, the endorectal coil is not commonly used in MRI examinations intended for radiation therapy treatment planning. Consequently, the signal-to-noise of the fMRI is not as good, leading to a reduced spatial resolution and sensitivity for detecting small lesions.

■ Detection limit

Prostate cancer is a heterogeneous disease that is often found with multiple tumor foci in the prostate. Chen *et al.* determined the volume and location of tumor foci in 180 prostatectomy specimens and found that 83% of the prostates had more than one tumor focus, with a median of three foci [61]. The volume of the tumors varied from 0.01 to 19.06 cc, with a median of 1.39 cc. Similar results were found recently by Bott *et al.* [62]. They showed that the median volume of the largest (index) tumor was 0.95 cc (range: 0.1–18.2 cc), whereas the median volume of the largest secondary tumor was 0.2 cc (range: 0.05–1.7 cc).

Schmuecking *et al.* investigated the detection level for lesion characterization in the prostate using DCE-MRI and MRSI [63]. In this study they used the commercially available MR sequences on a 1.5T scanner. While this study confirms the high sensitivity and specificity of DCE-MRI (82 and 89%, respectively) and somewhat lower values for MRSI (sensitivity: 68%; specificity: 67%), the study also demonstrated that prostatic intraepithelial neoplasia lesions are not detected by either technique. For DCE-MRI, lesions smaller than 3 mm and/or containing less than 30% cancer cells could not be detected. For MRSI the cut-off level was 4 mm and/or less than 40% tumor cell content. Consequently, in cases with diffuse tumor growth they found that the tumor volume tended to be underestimated when using these techniques.

A similar conclusion was drawn for DWI-MRI by Langer *et al.* in a study comparing tumors in histology with diffusion-weighted imaging and quantitative T_2-mapping [64]. Tumors in which more than 50% of their cross-sectional areas contained primarily normal peripheral zone tissue were designated as 'sparse' tumors. These tumors were found to have similar ADC and T_2 values to normal peripheral zone tissue, whereas in 'dense' tumors a lower ADC and T_2 were found. This implies that prostate tumors may hold regions that are intrinsically invisible with these imaging techniques, thereby limiting the accuracy of target delineation.

Within radiation therapy, the gross target volume (GTV) is used to identify the tumor that is visible to the radiation oncologist. The clinical target volume (CTV) is the volume containing 'subclinical' disease, for example a low density of tumor cells, below the detection threshold of the imaging techniques available. For application of fMRI techniques in radiotherapy, information about the detectability of small lesions and tumor volumes holding a low fraction of cancerous cells provides us with clues about the distinction between GTV and CTV. Typically, the dose required for control of the tumor depends on the density of tumor cells. Thus, information about the detection threshold is critical for improving our understanding of the dose requirements of visible tumors and the rest of the prostate.

■ Making delineation decisions based on a combination of MRI techniques

As described above, an MRI examination for staging prostate cancer preferably involves a combination of techniques. Where individual techniques may suffer from either a lower sensitivity (e.g., MRSI) or specificity (e.g., DCE-MRI), their combination results in a high accuracy for detecting and staging prostate cancer.

While combining different techniques is advantageous in a diagnostic setting, a problem emerges for tumor delineation: if different techniques show conflicting results about the presence of tumor, it is unclear which voxels should be included in the target volume. Even if multiple techniques indicate the presence of a tumor in a particular region of the prostate, the boundaries of this tumor may not be the same in all modalities.

Groenendaal *et al.* investigated if DCE-MRI and DWI provide consistent information on a voxel level [48]. Owing to uncertainty regarding

the precise threshold levels that would be optimal for distinguishing tumor from healthy tissue, a more sophisticated analysis of the images was performed. Based on the receiver operating characteristic analysis, the agreement of one imaging modality with a segmentation based on the other imaging modality was determined. This was carried out for a range of threshold values for ADC and K^{trans}. The results showed that the area under the curve (AUC) varied substantially between patients. Values of up to 0.90 were found in some patients, indicating that both imaging modalities identify the same volume as tumor. However, on average the AUC values were 0.60. Thus, in many patients only a partial overlap between the two modalities was seen. This shows that DCE-MRI and DWI provide complementary information and that the combination of modalities reflects heterogeneity in the cancerous tissue in the prostate.

While whole-mount section histology is required to validate the imaging modalities, in clinical practice uncertainty will remain on the interpretation of apparently inconsistent imaging data. A radiation oncologist will have to delineate tumors inside the prostate without having the ground truth of whole-mount section histology available. Therefore, a method is required to deal with this uncertainty. A practical approach is to classify the target volume according to risk. Following an approach proposed by the working group on gynecologic cancer of the Groupe Européen de Curiethérapie-European Society for Therapeutic Radiology and Oncology (GEC-ESTRO) [65], the GTV can be defined as the volume that is consistently identified as tumor on all imaging modalities. A high-risk CTV can be defined, which involves the voxels that are suspected based on some of the imaging modalities, but not consistently identified on all. The CTV can then be regarded as the volume of subclinical disease, not identified as suspicious by any of the imaging modalities [48,66]. In a focal boost treatment plan, the high-risk CTV essentially functions as a margin around the GTV, in which dose escalation is allowed, but not required (Figure 2).

■ Pathological validation

The gold standard for validation of imaging modalities is whole-mount section histology of prostatectomy specimen. To appreciate the impact of tumor heterogeneity on the images, a better understanding is required of the tissue properties that are detected in each of the imaging techniques. This calls for pathology studies of prostate cancer that do not primarily focus on the tumor location, but rather on properties such as cell density ('cellularity') and microvessel density. Particularly interesting are the regions that yield conflicting information from different imaging modalities. However, accurate validation of these techniques with a high spatial accuracy is very challenging. Processing and registration of the prostatectomy specimen needs to be very precise. Since the exact tumor location and extent are not as critical in a diagnostic setting, the validation of MR techniques has mainly been carried out on larger parts of the prostate, such as octants [29,30,45].

In particular, when an endorectal coil is used during imaging, the deformations of the prostate between images and histology slices can be large. Shah *et al.* proposed to improve the spatial correlation by placing the prostate specimen in a mold that was fabricated to match the *in vivo* shape of the prostate [67]. Specific care was taken to cut the tissue blocks in the same direction as the imaging slices.

Turkbey *et al.* applied two methods to correlate MR images to whole-mount section pathologic sections [68]. In the stringent approach, a one-to-one correlation was determined between imaging and pathologic findings. In an alternative approach, neighboring regions on the 3D grid were also included in the correlation, assuming that any displacement of a tumor focus due to distortions of the pathologic sections would be limited in distance. As expected, a significant increase in sensitivity and specificity was found when including the neighboring regions in the analysis.

Park *et al.* proposed a method to improve the spatial correlation between images and histology slices by breaking up the registration procedure in subregistration steps involving intermediate modalities [69]. To this end, each histology section is registered to a block face photograph of the prostate. A stack of block-face photographs, constituting an image of the prostate, is registered to an *ex vivo* MR image of the prostate taken after the prostatectomy. This image is finally registered onto the *in vivo* MRI of the prostate. Following this method, they found registration errors between histology and *in vivo* MRI data of 3.7 and 2.3 mm in two patients. Following a similar approach for five patients, Groenendaal *et al.* also found registration errors of 2–3 mm [70]. A comparison of delineations of tumors on MRI with pathology, showed that 85–100% of the tumor

was included in the delineated volume when a registration uncertainty of 3–5 mm was taken into account.

Future perspective

■ Methods for automatic segmentation based on multimodality MRI

The combination of conventional MRI with fMRI techniques is quite successful in differentiating benign and malignant prostate tissue. As a result, the use of fMRI techniques combined with T_2-weighted imaging is gaining recognition for staging of prostate cancer. For tumor delineation, some uncertainties still exist, in particular regarding cut-off levels for functional parameter maps and regarding the spatial resolution of these techniques.

To increase the robustness of the use of multiple imaging techniques, several groups have proposed an automated analysis of the images. Vos *et al.* use a support vector machine as a

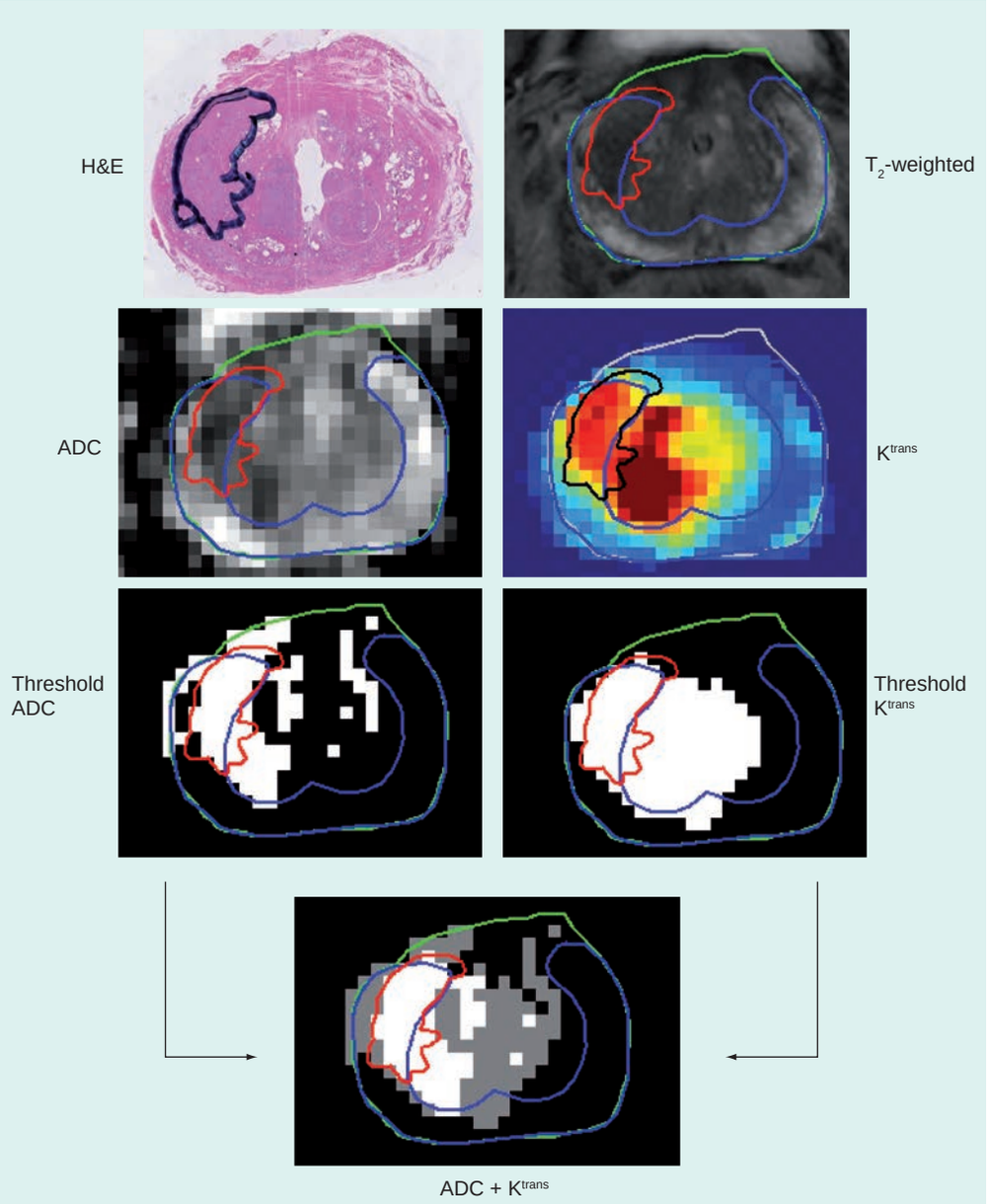

Figure 2. Pathology and imaging data of a patient with a tumor in the right lateral side of the peripheral zone. For the ADC a threshold of 1.1 × 10^{-3} mm^2/s was used, for K^{trans} a threshold of 0.18 min^{-1}. The bottom image shows in white the voxels where both modalities overlap, in gray the voxels where the modalities provide conflicting information. Black voxels are not suspicious of the presence of tumor.
ADC: Apparent diffusion coefficient.

classifier that is used as a measure of likelihood of malignancy [71]. The diagnostic accuracy (AUC) obtained for differentiating prostate cancer from nonmalignant disorders in the peripheral zone was 0.83. However, in radiotherapy, the challenge is the delineation of the tumor, rather than the diagnosis. Thus, for each voxel the radiation oncologist needs to decide if it is part of the tumor or not. In a voxelwise analysis of T_2-weighted MRI, DWI and DCE-MRI, Langer *et al.* used logistic regression to create an objective model for mapping tumors in the peripheral zone [72]. Ozer *et al.* took this work one step further and studied a variety of supervised and unsupervised learning methods to derive a segmentation of prostate tumors [73]. Their results show that supervised methods, such as support vector machines, perform better than unsupervised methods, particularly when a combination of MRI modalities is used. Nevertheless, the outcome of such tumor prediction models will have some remaining uncertainty, because of limitations in sensitivity and specificity [73] of the model as well as in repeatability of the MRI examinations. For application in radiotherapy, this remaining uncertainty must be incorporated in the target definition. As discussed above, this could again be carried out by explicitly identifying distinct risk levels [66]: voxels with a high risk of containing tumor could be identified as GTV. Voxels with a low risk of containing macroscopic tumor may hold microscopic disease and could be identified as CTV. For voxels with an intermediate risk, a high-risk CTV was proposed. When boosting the dose to the GTV, the high-risk CTV functions as a margin around the GTV, where a higher dose is allowed.

■ Testing the effectiveness of dose painting in the prostate

The evaluation of the effectiveness of dose painting in prostate cancer needs to be established in randomized clinical trials. To date, one Phase III trial has started [101]. Although such randomized trials are necessary, the 'classical' end points are not very strong for evaluating the effectiveness of the dose painting itself. In the experimental arm, the patients receive a higher dose than in the standard arm. Thus, even if the dose escalation is erroneously given in a location without tumor load, the tumor control in the experimental arm cannot be lower than in the standard arm. Similarly, the treatment-related toxicity cannot be lower.

To deal with this problem, it is important to investigate the precise location of a recurrence. In particular if a recurrence is local, it is important to establish what the dose level was at that precise location. Van Vulpen *et al.* showed the feasibility of this approach in a study of 14 patients, treated with external-beam radiotherapy and brachytherapy [74].

Several MRI techniques have been proposed to image local recurrences in prostate cancer, as reviewed by De Visschere *et al.* [75]. Follow-up imaging after radiotherapy needs to take into account the fact that many changes occur in the prostate, that are not related to outcome, such as inflammation, glandular atrophy, fibrosis and prostate shrinkage [75]. In particular, MRSI shows a clear benefit for prostate cancer follow-up after treatment [76,77]. In a few studies on DCE-MRI in localizing local recurrences, a superiority of DCE-MRI over T_2-weighted MRI was shown. In patients with a history of radiotherapy contrast, DCE imaging offers a favorable contrast between the early enhancing recurrence and the slowly enhancing postradiation fibrosis [78,79].

■ Imaging tumor aggressiveness & radiosensitivity

For guiding the clinical choices regarding dose to the tumor for individual patients, it is important to identify which tumors require a high dose and for which tumors the current dose of approximately 78 Gy would suffice. Properties such as cell density and microvessel density are likely to have an impact on tumor radiosensitivity. Several studies present evidence of the correlation of choline-containing compounds in prostate tumors and their aggressiveness [80,81]. Biopsy studies also revealed altered levels of polyamine metabolites, suggesting a negative correlation between polyamines and Gleason score [80]. A qualitative assessment of polyamines has been performed *in vivo* by MRSI at 1.5T [82]. Evidence is also emerging that ADC values reflect Gleason score. Tamada *et al.* found a significant negative, although not very strong correlation, between ADC in the peripheral zone and the Gleason score (rho = -0.497; p = 0.001) [83]. Similar results were also found by Yoshimitsu *et al.* [84].

Hypoxia is another important factor in determining the radiosensitivity of a tumor. While DCE-MRI reflects the properties of the vasculature, blood oxygen-level dependent MRI has been tested in prostate to characterize the oxygenation in the tumor more

directly. Hoskin *et al.* used multiple gradient-recalled echo images at varying echo times to calculate an R_2* map [85]. In combination with estimates of the blood volume from dynamic susceptibility contrast MRI, this was used to assess the oxygenation of prostate tissue. Nevertheless, the interpretation of these data remains difficult.

Chopra *et al.* also showed a correlation between R_2* and hypoxia measurements using a polarographic needle electrode [86]. However, they also found a strong correlation between R_2* and T_2, concluding that further development is required to extract oxygenation effects robustly from tissue signal relaxation metrics.

When the value of these functional imaging modalities is established for characterizing tumor aggressiveness and radiosensitivity, they can be expected to play an important role in selection of the most appropriate dose range, optimizing the balance between the risk of toxicity and the likelihood of achieving tumor control.

Conclusion

The value of fMRI techniques for detecting prostate cancer is now well established within the radiology community. The potential of these techniques is also beginning to receive recognition within the radiation therapy community, as indicated by the various planning studies on focal boosting of prostate tumors. Nevertheless, their application in clinical practice is still limited to a few institutes, mainly within research hospitals. Tumor delineation is currently a manual procedure, where a radiation oncologist and radiologist decide what to include in the target, based on the available images and clinical information.

For a more widespread application, it seems that the robustness of the techniques must be improved. As prostate cancer is a multifocal disease, the optimal spatial resolution needs to be established at which fMRI techniques can be used for tumor delineation. Repeatability studies that study the variation of imaging parameter maps at a voxel level are required. As data from

Executive summary

Functional MRI techniques for tumor delineation in radiation therapy

- The potential of functional MRI techniques for tumor delineation has begun to receive recognition within the radiation therapy community, as indicated by the various planning studies on focal boosting of prostate tumors.
- The toxicity and effectiveness of dose painting in prostate radiation therapy is being tested in clinical trials.
- When patients are scheduled for radiation therapy, the presence of prostate cancer has been proven with biopsies and the stage of the disease has been established. Thus, rather than a qualitative assessment of location or capsular extension of the tumor, the precise boundaries of the lesions inside the prostate must be determined for target delineation.
- Tumor delineation essentially means that for each voxel a decision has to be made if it is part of the target volume or not.

Detection limits

- Several studies have determined detection limits for dynamic contrast-enhanced MRI and diffusion-weighted MRI. Detectability depends not only on size, but also the percentage of cancerous cells within a volume.
- In radiation therapy, sparse tumors may require a lower dose than dense tumors.

Repeatability & spatial resolution

- For tumor delineation we need to know what voxel sizes can be used meaningfully for making delineation decisions. Therefore, the repeatability of functional MRI examinations must be established as a function of voxel size.
- For dynamic contrast-enhanced CT, voxels of 0.15 cc showed a within-standard deviation of K^{trans} of 0.047 min^{-1}, which is sufficient to discriminate tumor from healthy tissue. At least a similar spatial resolution should be feasible for MRI.

Delineation decisions based on a combination of MRI techniques

- Owing to tumor heterogeneity, different MRI techniques may show conflicting results about the presence of tumor in a voxel. In these cases it is unclear which voxels to include in the target volume.
- A pragmatic approach to deal with this uncertainty is to classify multiple target volumes according to risk. In a focal boost treatment plan, the intermediate risk target volume essentially forms a margin around the high-risk tumor volume.
- Owing to tumor heterogeneity, validation of (combinations of) imaging modalities must be carried out at a high spatial resolution. However, as the registration accuracy between histology and imaging data sets is currently limited to 2–3 mm, the validation of even smaller features in images is not feasible.

Future perspective

- For a more widespread application of functional MRI techniques for delineation of prostate tumors, the robustness of these techniques must be improved. Automated analysis of imaging, using support vector machines or logistic regression models may be helpful for this purpose.
- To test the effectiveness of dose painting in clinical trials, it is important to correlate the precise location of a recurrence with the original location of the tumor as well as the given radiation dose. Therefore, diagnostic techniques for locally recurrent prostate cancer are essential.

multiple MRI techniques reflect tumor heterogeneity, validation of this heterogeneity with pathology is required to identify which parts of the suspected volumes should be included in the target volume for boosting the radiation dose. Relatively simple methods to deal with this heterogeneity, such as the use of target volumes for different risk levels, need to be improved by using automated methods to translate multiparametric data into appropriate segmentations.

In conclusion, fMRI techniques for delineating prostate cancer are now being used in radiation therapy dose painting. At least one randomized Phase III trial is currently under way to investigate the benefit of a focal boost to the visible tumor inside the prostate [101]. Nevertheless, to expand the use of fMRI techniques beyond a limited number of research centers, their robustness needs to be improved.

Financial & competing interests disclosure

This work was funded by Dutch Cancer Society grants KWF2007–3893, KWF 2009–4310 and KWF 2009–4500. The authors have no other relevant affiliations or financial involvement with any organization or entity with a financial interest in or financial conflict with the subject matter or materials discussed in the manuscript apart from those disclosed.

No writing assistance was utilized in the production of this manuscript.

Bibliography

Papers of special note have been highlighted as:
▪▪ of considerable interest

1 Pollack A, Zagars GK, Starkschall G *et al.*: Prostate cancer radiation dose response: results of the MD Anderson Phase III randomized trial. *Int. J. Radiat. Oncol. Biol. Phys.* 53, 1097–1105 (2002).

2 Zietman AL, DeSilvio ML, Slater JD *et al.*: Comparison of conventional-dose vs high-dose conformal radiation therapy in clinically localized adenocarcinoma of the prostate: a randomized controlled trial. *JAMA* 294, 1233–1239 (2005).

3 Peeters ST, Heemsbergen W, Koper PC *et al.*: Dose–response in radiotherapy for localized prostate cancer: results of the Dutch multicenter randomized Phase III trial comparing 68 Gy of radiotherapy with 78 Gy. *J. Clin. Oncol.* 24, 1990–1996 (2006).

4 Lips IM, Dehnad H, Van Gils CH, Boeken-Kruger AE, Van der Heide UA, Van Vulpen M: High dose intensity-modulated radiotherapy for prostate cancer using daily fiducial marker-based position verifcation: acute and late toxicity in 331 patients. *Radiat. Oncol.* 3, 15 (2008).

5 Lips IM, van Gils CH, van der Heide UA, Boeken Kruger UA, van Vulpen M: Health-related quality of life 3 years after high-dose intensity-modulated radiotherapy with gold fiducial marker-based position verification. *BJU Int.* 103, 762–767 (2009).

6 Cellini N, Morganti AG, Mattiucci GC *et al.*: Analysis of intraprostatic failures in patients treated with hormonal therapy and radiotherapy: implications for conformal therapy planning. *Int. J. Radiat. Oncol. Biol. Phys.* 53, 595–599 (2002).

7 Pucar D, Sella T, Schöder H *et al.*: The role of imaging in the detection of prostate cancer local recurrence after radiation therapy and surgery. *Curr. Opin. Urol.* 18, 87–97 (2008).

8 Pickett B, Vigneault E, Kurhanewicz J, Verhey L, Roach M: Static field intensity modulation to treat a dominant intra-prostatic lesion to 90 Gy compared with seven field 3-dimensional radiotherapy. *Int. J. Radiat. Oncol. Biol. Phys.* 44, 921–929 (1999).

9 De Meerleer G, Villeirs G, Bral S *et al.*: The magnetic resonance detected intraprostatic lesion in prostate cancer: planning and delivery of intensity-modulated radiotherapy. *Radiother. Oncol.* 75, 325–333 (2005)

10 Van Lin EN, Futterer JJ, Heijmink SW *et al.*: IMRT boost dose planning on dominant intraprostatic lesions: gold marker-based three-dimensional fusion of CT with dynamic contrast-enhanced and 1H-spectroscopic MRI. *Int. J. Radiat. Oncol. Biol. Phys.* 65, 291–303 (2006).

11 Pinkawa M, Holy R, Piroth MD *et al.*: Intensity-modulated radiotherapy for prostate cancer implementing molecular imaging with 18F-choline PET-CT to define a simulteneous integrated boost. *Strahlenth. Onkol.* 186, 600–606 (2010).

12 Bentzen SM: Theragnostic imaging for radiation oncology: dose-painting by numbers. *Lancet Oncol.* 6, 112–117 (2005).

13 Ennis RD: Potential benefits of intra-prostatic cancer-specific imaging to guide therapy and monitor outcome in patients treated with radiation-based treatments for localized prostate cancer. *Cancer Biomark.* 4, 197–199 (2008).

▪▪ **Compact introduction to the potential of dose painting in radiation therapy in comparison to other treatment modalities, and the role of imaging.**

14 Fonteyne V, Villeirs G, Speleers B, *et al.*: Intensity-modulated radiotherapy as primary therapy for prostate cancer: report on acute toxicity after dose escalation with simultaneous integrated boost to intraprostatic lesion. *Int. J. Radiat. Oncol. Biol. Phys.* 72, 799–807 (2008).

15 Singh AK, Guion P, Sears-Crouse N *et al.*: Simultaneous integrated boost of biopsy proven, MRI defined dominant intra-prostatic leasions to 95 Gy with IMRT: early results of a phase I NCI study. *Radiat. Oncol.* 2, 36 (2007).

16 Trotti A, Byhardt R, Stez J *et al.*: Common toxicity criteria: version 2.0. an improved reference for grading the acute effects of cancer treatment: impact on radiotherapy. *Int. J. Radiat. Oncol. Biol. Phys.* 47, 13–47 (2000).

17 Rasch C, Steenbakkers R, Van Herk M: Target definition in prostate, head, and neck. *Semin. Radiat. Oncol.* 15, 136–145 (2005).

18 McLaughlin PW, Troyer S, Berri S *et al.*: Functional anatomy of the prostate: implications for treatment planning. *Int. J. Radiat. Oncol. Biol. Phys.* 63, 479–491 (2005).

19 Villeirs GM, Verstraete K, De Neve WJ, De Meerleer GO: Magnetic resonance imaging anatomy of the prostate and periprostatic area: a guide for radiotherapists. *Radiother. Oncol.* 76, 99–106 (2005).

20 Rosewall T, Kong V, Vesprini D *et al.*: Prostate delineation using CT and MRI for radiotherapy patients with bilateral hip prostheses. *Radiother. Oncol.* 90, 325–330 (2009).

21 Hricak H, Choycke PL, Eberhardt SC, Leibel SA, Scardino PT: Imaging prostate cancer: a multidisciplinary perspective. *Radiology* 243, 28–53 (2007).

22 Fuchsjäger M, Shukla-Dave A, Akin O, Barentsz J, Hricak H: Prostate cancer imaging. *Acta Radiol.* 49, 107–120 (2008).

23 Seitz M, Shukla-Dave A, Bjartell A *et al.*: Functional magnetic resonance imaging in prostate cancer. *Eur. Urol.* 55, 801–814 (2009).

24 Kirkham AP, Emberten M, Allen C: How good is MRI at detecting and characterising cancer within the prostate? *Eur. Urol.* 50, 1163–1174 (2006).

25 Fütterer JJ, Heijmink SW, Scheenen TW *et al.*: Prostate cancer: local staging at 3-T endorectal MR imaging – early experience. *Radiology* 238, 184–191 (2006).

26 Hara N, Okuizumi M, Koike H, Kawaguchi M, Bilim V: Dynamic contrast-enhanced magnetic resonance imaging (DCE-MRI) is a useful modality for the precise detection and staging of early prostate cancer. *Prostate* 62, 140–147 (2005).

27 Kim JK, Hong SS, Choi YJ *et al.*: Wash-in rate on the basis of dynamic contrast-enhanced MRI: usefulness for prostate cancer detection and localization. *J. Magn. Reson. Imaging* 22, 639–646 (2005).

28 Tofts PS, Brix G, Buckley DL *et al.*: Estimating kinetic parameters from dynamic contrast-enhanced T_1-weighted MRI of a diffusable tracer: standardized quantities and symbols. *J. Magn. Reson. Imaging* 10, 223–232 (1999).

29 Fütterer JJ, Heijming SWTPJ, Scheenen TWJ *et al.*: Prostate cancer localization with dynamic contrast-enhanced MR imaging and proton MR spectroscopic imaging. *Radiology* 241, 449–458 (2006).

30 Van Dorsten FA, Van der Graaf M, Engelbrecht MRW *et al.*: Combined quantitative dynamic contrast-enhanced MR imaging and ^{1}H MR spectroscopic imaging of human prostate cancer. *J. Magn. Reson. Imaging* 20, 279–287 (2004).

31 Hom JJ, Coakley FV, Simko JP *et al.*: Prostate cancer: endorectal MR imaging and MR spectroscopic imaging – distinction of true-positive results from chance-detected lesions. *Radiology* 238, 192–199 (2006).

32 Shimofusa R, Fujimoto H, Akamata H *et al.*: Diffusion-weighted imaging of prostate cancer. *J. Comput. Assist. Tomogr.* 29, 149–153 (2005).

33 DeSouza NM, Reinsberg SA, Scurr ED, Brewster ED Payne GS: Magnetic resonance imaging in prostate cancer: the value of apparent diffusion coefficients for identifying malignant nodules. *Br. J. Radiol.* 80, 90–95 (2007).

34 Morgan VA, Kyriazi S, Ashley SE, deSouza NM: Evaluation of the potential of diffusion-weighted imaging in prostate cancer detection. *Acta. Radiol.* 48, 695–703 (2007).

35 Haider MA, van der Kwast TH, Tanguay J *et al.*: Combined T_2-weighted and diffusion-weighted MRI for localization of prostate cancer. *AJR Am J Roentgenol.* 189, 323–328 (2007).

36 Tanimoto A, Nakashima J, Kohno H, Shinmoto H, Kuribayashi S: Prostate cancer screening: the clinical value of diffusion-weighted imaging and dynamic MR imaging in combination with T_2-weighted imaging. *J. Magn. Reson. Imaging.* 25, 146–152 (2007).

37 Yoshimitsu K, Kiyoshima K, Irie H *et al.*: Usefulness of apparent diffusion coefficient map in diagnosing prostate carcinoma: correlation with stepwise histopathology. *J. Magn. Reson. Imaging.* 27, 132–139 (2008).

38 Mazaheri Y, Shukla-Dave A, Muellner A, Hricak H: MR imaging of the prostate in clinical practice. *MAGMA* 21, 379–392 (2008).

39 Chen M, Dang HD, Wang JY *et al.*: Prostate cancer detection: comparison of T_2-weighted imaging, diffusion-weighted imaging, proton magnetic resonance spectroscopic imaging, and the three techniques combined. *Acta Radiol.* 49, 602–610 (2008).

40 Alonzi R, Padhani AR, Taylor NJ *et al.*: Antivascular effects of neoadjuvant androgen deprivation for prostate cancer: an *in vivo* human study using susceptibility and relaxivity dynamic MRI. *Int. J. Radiat. Oncol. Biol. Phys.* DOI:10.1016/j.ijrobp.2010.02.060 (2011) (Epub ahead of print).

41 Padhani AR, Hayes C, Landau S, Leach MO: Reproducibility of quantitative dynamic MRI of normal human tissues. *NMR Biomed.* 15, 143–153 (2002).

42 Kershaw LE, Hutchinson CE, Buckley DL: Benign prostate hyperplasia: evaluation of T_1, T_2 and microvascular characteristics with T_1-weighted dynamic contrast-enhanced MRI. *J. Magn Reson. Imaging* 29, 641–648 (2009).

43 Parker GJ, Roberts C, Macdonald A, *et al.*: Experimentally-derived functional form for a population-averaged high-temporal-resolution arterial input function for dynamic contrast-enhanced MRI. *Magn. Reson. Med.* 56, 993–1000 (2006).

44 Buckley DL, Roberts C, Parker JP, Hutchinson CE: Prostate cancer: Evaluation of vascular characteristics with dynamic contrast-enhanced T_1-weighted MR imaging – initial experience. *Radiology* 233, 709–715 (2004).

45 Kozlowski P, Chang SD, Jones EC, Berean KW, Chen H, Goldenberg SL: Combined diffusion-weighted and contrast-enhanced MRI for prostate cancer diagnosis – correlation with biopsy and histopathology. *J. Magn. Reson. Imaging* 24, 108–113 (2006).

46 Ocak I, Bernardo M, Metzger G *et al.*: Dynamic contrast-enhanced MRI of prostate cancer at 3T: a study of pharmacokinetic parameters. *Am. J. Roentgenol.* 189, W192–W201 (2007).

47 Alonzi R, Taylor NJ, Stirling JJ *et al.*: Reproducibility and correlation between quantitative and semiquantitative dynamic and intrinsic susceptibility-weighted MRI parameters in the benign and malignant human prostate. *J. Magn. Reson. Imaging* 32, 155–164 (2010).

48 Groenendaal G, Van den Berg CAT, Korporaal JG *et al.*: Simulatenous MRI diffusion and perfusion imaging for tumor delineation in prostate cancer patients. *Radiother. Oncol.* 95, 185–190 (2010).

49 Kozlowski P, Chang SD, Meng R *et al.*: Combined prostate diffusion tensor imaging and dynamic contrast-enhanced MRI at 3T – quantitative correlation with biopsy. *Magn. Reson. Imaging* 28, 621–628 (2010).

50 Langer DL, Van der Kwast TH, Evans AJ *et al.*: Prostate tissue composition and MR measurements: investigating the relationships between ADC, T_2, K^{trans}, v^e, and corresponding histologic features. *Radiology* 255, 485–494 (2010).

51 Henderson E, Milosevic MF, Haider MA, Yeung IWT: Functional CT imaging of prostate cancer. *Phys. Med. Biol.* 48, 3085–3100 (2003).

52 Jeukens CR, Van den Berg CA, Donker R *et al.*: Feasibility and measurement precision of 3D quantitative blood flow mapping of the prostate using dynamic contrast-enhanced multi-slice CT. *Phys. Med. Biol.* 51, 4329–4343 (2006).

53 Korporaal JG, van den Berg CAT, Jeukens CRLPN *et al.*: Dynamic contrast-enhanced CT for prostate cancer: relationship between image noise, voxel size, and repeatability. *Radiology* 256, 976–984 (2010).

▪▪ **Addresses the spatial resolution at which data from dynamic contrast-enhanced CT can be applied for tumor delineation.**

54 Gibbs P, Pickles MD, Turnbull LW: Repeatability of echo-planar-based diffusion measurements of the human prostate at 3T. *Magn. Reson. Imaging* 25, 1423–1429 (2007).

55 Padhani AR, Liu G, Koh DM *et al.*: Diffusion-weighted magnetic resonance imaging as a cancer biomarker: consensus and recommendations. *Neoplasia* 11, 102–125 (2009).

56 Scheenen TWJ, Heijmink SWTPJ, Roell SA *et al.*: Three-dimensional proton MR spectroscopy of human prostate at 3T without endorectal coil: feasibility. *Radiology* 245, 507–516 (2007).

57 Heijmink SWTPJ, Fütterer JJ, Hambrock T *et al.*: Prostate cancer: body-array versus endorectal coil MR imaging at 3T – comparison of image quality, localization, and staging. *Radiology* 244, 184–195 (2007).

58 Heijmink SWTPJ, Scheenen TWJ, Van Lin ENJT *et al.*: Changes in prostate shape and volume and their implications for radiotherapy after introduction of endorectal balloon as determined by MRI at 3T. *Int. J. Radiat. Oncol. Biol. Phys*. 73, 1446–1453 (2009).

59 Kim Y, Hsu IC, Pouliot J, Noworolski SM, Vigneron DB, Kurhanewicz J: Expandable and rigid endorectal coils for prostate MRI: impact on prostate distortion and rigid image registration. *Med. Phys.* 32, 3569–3578 (2005).

60 Woel R, Beard C, Chen M-H *et al.*: Acute gastrointestinal, genetourinary, and dermatological toxicity during dose-escalated 3D-conformal radiation therapy (3DCRT) using an intrarectal balloon for prostate gland localization and immobilization. *Int. J. Radiat. Oncol. Biol. Phys*. 62, 392–396 (2005).

61 Chen ME, Johnston DA, Tang K, Babaian RJ, Troncoso P: Detailed mapping of prostate carcinoma foci. Biopsy strategy implications. *Cancer* 89, 1800–1809 (2000).

62 Bott SRJ, Ahmed HU, Hindley RG, Abdul-Rahman A, Freeman A, Emberton M: The index lesion and focal therapy: an analysis of pathologic characteristics of prostate cancer. *BJU Int*. 106, 1607–1611 (2010).

63 Schmuecking M, Boltze C, Geyer H *et al.*: Dynamic MRI and CAD vs. choline MRS: where is the detection level for a lesion characterisation in prostate cancer? *Int. J. Radiat. Biol.* 85, 814–824 (2009).

▪▪ **Discusses the application of functional MRI techniques for tumor delineation in radiation therapy treatment planning.**

64 Langer DL, Van der Kwast TH, Evans AJ *et al.*: Intermixed normal tissue within prostate cancer: effect on MR imaging measurements of apparent diffusion coefficient and T_2 – sparse versus dense cancers. *Radiology* 249, 900–908 (2008).

▪▪ **Discusses the capacity of diffusion-weighted MRI to detect tumors with different percentages of cancerous cells.**

65 Haie-Meder C, Pötter R, Van Limbergen E *et al.*: Recommendations from gynaecological (GYN) GEC-ESTRO Working Group (I): concepts and terms in 3D image based 3D treatment planning in cervix cancer brachytherapy with emphasis on MRI assessment of GTV and CTV. *Radiother. Oncol.* 74, 235–245 (2005).

66 Korporaal JG, Van den Berg CAT, Groenendaal G, Moman MR, Van Vulpen M, Van der Heide UA: The use of probability maps to deal with the uncertainties in prostate cancer delineation. *Radiother. Oncol.* 94, 168–172 (2010).

67 Shah V, Pohida T, Turkbey B *et al.*: A method for correlating *in vivo* prostate magnetic resonance imaging and histopathology using individualized magnetic resonance-based molds. *Rev. Sci. Instrum.* 80, 104301 (2009).

68 Turkbey B, Pinto PA, Mani H *et al.*: Prostate cancer: value of multiparametric MR imaging at 3T for detection – histopathologic correlation. *Radiology* 255, 89–99 (2010).

69 Park H, Piert MR, Khan A *et al.*: Registration methodology for histological sections and in-vivo imaging of human prostate. *Acad. Radiol.* 15, 1027–1039 (2008).

70 Groenendaal G, Moman MR, Korporaal JG *et al.*: Validation of functional imaging with pathology for tumor delineation in the prostate. *Radiother. Oncol.* 94, 145–150 (2010).

71 Vos PC, Hambrock T, Hulsbergen-van de Kaa CA, Fütterer JJ, Barentsz JO, Huisman JJ: Computerized analysis of prostate lesions in the peripheral zone using dynamic contrast enhanced MRI. *Med. Phys.* 35, 888–899 (2008).

72 Langer DL, Van der Kwast TH, Evans AJ, Trachtenberg J, Wilson BC, Haider MA: Prostate cancer detection with multi-parametric MRI: logistic regression analysis of quantitative T_2, diffusion-weighted imaging, and dynamic contrast-enhanced MRI. *J. Magn. Reson. Imaging* 30, 327–334 (2009).

73 Ozer S, Langer DL, Liu X *et al.*: Supervised and unsupervised methods for prostate cancer segmentation with multispectral MRI. *Med. Phys.* 37, 1873–1883 (2010).

74 Van Vulpen M, Van den Berg CAT, Moman MR, Van der Heide UA: Difficulties and potential of correlating local recurrences in prostate cancer with the delivered local dose. *Radiother. Oncol.* 93, 180–184 (2009).

75 De Visschere PJ, De Meerleer GO, Fütterer JJ, Villeirs GM: Role of MRI in follow-up after focal therapy of prostate carcinoma. *Am. J. Roentgenol.* 194, 1427–1433 (2010).

76 Pucar D, Shukla-Dave A, Hricak H *et al.*: Prostate cancer: correlation of MR imaging and MR spectroscopy with pathologic findings after radiation therapy – initial experience. *Radiology* 236, 545–553 (2005).

77 Westphalen AC, Coakley FV, Roach III M, McCulloch CE, Kurhanewicz J: Locally recurrent prostate cancer after external beam radiation therapy: diagnostic performance of 1.5-T endorectal MR imaging and MR spectroscopic imaging for detection. *Radiology* 256, 485–492 (2010).

78 Rouviere O, Valette O, Grivolat S *et al.*: Recurrent prostate cancer after external beam radiotherapy: value of contrast-enhanced dynamic MRI in localizing intraprostatic tumor – correlation with biopsy findings. *Urology* 63, 922–927 (2004).

79 Haider MA, Chung P, Sweet J *et al.*: Dynamic contrast-enhanced magnetic resonance imaging for localization of recurrent prostate cancer after external beam radiotherapy. *Int. J. Radiat. Oncol. Biol. Phys.* 70, 425–430 (2008).

80 Swanson MG, Vigneron DB, Tabatabai ZL *et al.*: Proton HR-MAS spectroscopy and quantitative pathologic analysis of MRI/3D-MRSI-targeted postsurgical prostate tissues. *Magn. Reson. Med.* 50, 944–954 (2003).

81 Zakian KL, Sircar K, Hricak *et al.*: Correlation of proton MR spectroscopic imaging with gleason score based on step-section pathologic analysis after radical prostatectomy. *Radiology* 234, 804–814 (2005).

82 Shukla-Dave A, Hricak H, Moskowitz C *et al.*: Detection of prostate cancer with MR spectroscopic imaging: an expanded paradigm incorporating polyamines. *Radiology* 245, 499–506 (2007).

83 Tamada T, Sone T, Jo Y *et al.*: Apparent diffusion coefficient values in peripheral and transition zones of the prostate: comparison between normal and malignant prostatic tissues and correlation with histologic grade. *J. Magn. Reson. Imaging* 28, 720–726 (2008).

84 Yoshimitsu K, Kiyoshima K, Irie H *et al.*: Usefulness of apparent diffusion coefficient map in diagnosing prostate carcinoma: correlation with stepwise histopathology. *J. Magn. Reson. Imaging* 27, 132–139 (2008).

85 Hoskin PJ, Carnell DM, Taylor NJ *et al.*: Hypoxia in prostate cancer: correlation of BOLD-MRI with pimonidazole immunohistochemistry – initial observations. *Int. J. Radiat. Oncol. Biol. Phys.* 68, 1065–1071 (2007).

86 Chopra S, Foltz W, Milesovic MF *et al.*: Comparing oxygen-sensitive MRI (BOLD R_2*) with oxygen electrode measurements: a pilot study in men with prostate cancer. *Int. J. Radiat. Biol.* 85, 805–813 (2009).

■ Website

101 ClinicalTrials.gov: FLAME: investigate the benefit of a focal lesion ablative microboost in prostate cancer www.ClinicalTrials.gov